Original Article

대한치과재료학회지 51(3) : 129-144, 2024
Korean Journal of Dental Materials (*Korean J Dent Mater*)
ISSN:2384-4434 (Print); 2384-3268 (Online)
Available online at http://www.kadm.org
http://dx.doi.org/10.14815/kjdm.2024.51.3.129

임플란트용 티타늄의 표면 특성과 생체 적합성에 대한 MoS_2/폴리도파민 코팅 효과

유민서[1], 송요한[2], 한미경[1,*]

[1]전남대학교 공과대학 신소재공학부
[2]광주과학기술원(GIST) 화학과

Effect of MoS_2/polydopamine coating on surface properties and biocompatibility of Ti implants

Minseo Yu[1], Yo Han Song[2], Mi-Kyung Han[1,]*

[1]*Department of Materials Science and Engineering, Chonnam National University, Gwangju, Republic of Korea*
[2]*Department of Chemistry, Gwangju Institute of Science and Technology (GIST), Gwangju, Republic of Korea*

본 연구는 티타늄(Ti) 임플란트에서 몰리브덴 이황화물(MoS_2) 코팅의 접착력, 표면특성 및 부식 저항성을 향상시키기 위해 중간층으로서 폴리도파민(PDA)의 역할을 조사하였다. 이를 위해 Ti 표면에 PDA 처리를 한 후 MoS_2 코팅을 한 샘플과 Ti에 직접 MoS_2 코팅을 한 샘플을 비교 분석하였다. 표면 특성 분석은 X선 회절(XRD), X선 광전자 분광법(XPS), 라만 분광법 및 주사 전자 현미경(SEM)을 사용하여 종합적으로 수행되었다. 라만 분광법 및 SEM 분석 결과에 따르면, PDA 층은 더 균일하고 미세한 구조의 MoS_2 코팅을 촉진하는 것으로 나타났다. 습윤성 테스트에서는 MoS_2-PDA 처리된 표면이 직접 MoS_2 코팅된 표면보다 향상된 친수성을 보였다. 전위 동적 분극을 이용한 부식 저항성 테스트 결과, MoS_2-PDA 처리된 샘플이 직접 MoS_2 코팅된 샘플보다 낮은 부식 전류 밀도와 더 높은 부식 전위를 나타냈다. 세포 생존율 분석에서는 MoS_2-PDA 처리된 표면과 직접 MoS_2 코팅된 표면 모두 유사한 생체적합성을 보였으나, 세포 적합성에서는 MoS_2 군이 약간 더 높은 결과를 보였다. 이러한 결과는 PDA 중간층이 구조적 및 표면 특성을 향상시키는 반면, 두 접근법 간의 생체적합성 차이에 대한 더 많은 연구가 필요함을 시사한다. PDA 중간층은 여전히 표면 특성과 부식 저항성을 향상시키는 데 있어 정형외과 응용에서 잠재력을 보이고 있다.

색인단어 : MoS_2 코팅, 도파민, 젖음성, 세포 생존율, 티타늄 치과용 임플란트

Minseo Yu (ORCID: 0009-0006-1801-3020)
Yo Han Song (ORCID: 0000-0001-7521-4757)

*Correspondence: Mi-Kyung Han (ORCID: 0000-0003-1434-1562)
77, Yongbong-ro, Buk-gu, Gwangju 61186, Republic of Korea
Affiliation: Department of Materials Science & Engineering, Chonnam National University, Republic of Korea
Tel: +82-62-530-0450
E-mail: mikihan@jnu.ac.kr

Received: Jul. 17, 2024; Revised: Aug. 21, 2024; Accepted: Aug. 23, 2024

Introduction

Titanium (Ti) implants are widely used in dental and orthopedic applications due to their mechanical strength and biocompatibility (1). However, despite these advantages, the bioinert nature of Ti often hinders optimal tissue integration, leading to potential complications such as bacterial infections and implant failures (2, 3). One of the most significant challenges is the formation of biofilms on implant surfaces, which can cause persistent infections and complicate treatment outcomes (4-7). Recent advancements in nanomaterial coatings, particularly 2D materials like graphene and transition metal dichalcogenides such as molybdenum disulfide (MoS_2), have shown promise in addressing these issues (8-11). These materials exhibit antibacterial properties through various mechanisms, including physical disruption of microbial cell membranes, oxidative stress induced by reactive oxygen species (ROS), and photothermal effects under near-infrared (NIR) light (7, 12-15). MoS_2, in particular, has garnered attention for its high NIR absorption and efficient photothermal conversion, making it a strong candidate for enhancing the antibacterial properties of Ti implants (16-18).

However, applying MoS_2 coatings on Ti implants presents several challenges. Traditional methods such as spin-coating, chemical vapor deposition, and hydrothermal synthesis often result in inconsistent coating thicknesses and poor adhesion, undermining the long-term effectiveness of the implants (19-22). Ensuring durable and robust adhesion of MoS_2 to Ti substrates is, therefore, a critical objective.

Polymers like polydopamine (PDA), chitosan, polyurethanes (PU), poly(methacrylic acid) (PMMA), and poly(ethylene glycol) (PEG) have been explored for their potential to inhibit bacterial adhesion (23-26). Among these, PDA, inspired by the adhesive proteins of mussels, can adhere to nearly all solid surfaces through its catechol groups. Its ability to bind with metal ions, combined with its biocompatibility and biodegradability, makes it an excellent candidate for surface modification of Ti implants (27). Notably, PDA coating on Ti significantly improves corrosion resistance, hydrophilicity and bioactivity, promoting better cell adhesion and growth (28). Moreover, PDA on the surface of MoS_2 has been shown to enhance biocompatibility and photothermal properties (29).

Research has highlighted significant differences in photocurrent generation and Schottky barrier height between graphene/MoS_2 and Ti/MoS_2 interfaces (30). Specifically, the Schottky barrier at the Ti/MoS_2 interface is higher than at the graphene/MoS_2 interface, affecting charge transfer efficiency. Lowering the Schottky barrier can enhance charge transfer, which is beneficial for photothermal and photodynamic dental treatments by improving photothermal conversion and increasing the generation of reactive oxygen species (ROS). PDA possesses an exceptional photothermal conversion efficiency of about 40% (31). Therefore, it is hypothesized that introducing PDA between Ti and MoS_2 could modulate the work function and lower the Schottky barrier, thereby potentially improving the electronic properties and making the Ti/PDA/MoS_2 system more efficient for various applications, including dental treatments.

In this study, we investigate the effectiveness of combining MoS_2 and PDA coatings on Ti implants. We compare the biocompatibility and stability of MoS_2 coatings applied directly to Ti surfaces with those pre-treated with PDA. Extensive characterization of these coatings was conducted using X-ray diffraction (XRD), X-ray photoelectron spectroscopy (XPS), Raman spectroscopy, and scanning electron microscopy (SEM). Additionally, assessments of wettability, cell viability, corrosion resistance are performed to evaluate the overall efficacy and biocompatibility of the coatings.

Materials and Methods

1. Materials

The chemicals used in this study, dopamine hydrochloride, tris(hydroxymethyl)-aminomethane (Tris), sodium molybdate dihydrate ($Na_2MoO_4{\cdot}2H_2O$), and thioace-tamide (C_2H_5NS) were purchased from Sigma-Aldrich (St. Louis, MO, USA) and used without further purification. All the experiments were conducted using deionized water.

2. Pretreatment of Ti surface

Ti plates (ASTM Grade 2, Daito Steel Co. Ltd., Tokyo, Japan) were methodically polished using silicon carbide (SiC) sandpaper with progressively finer grains (#400, #600, #800, and #1200). Following the polishing process, the Ti plates were rinsed with acetone, ethanol and deionized water to ensure the removal of contaminants. Subsequently, the Ti plates underwent hydrothermal treatment in 4 M KOH at 85 ℃ for 2 hours. These treated substrates are designated as **OH@Ti**.

3. Preparation of PDA coating

For preparing the polydopamine (PDA) solution, dopamine was dissolved at a concentration of 2 mg/mL in 10 mM Tris-HCl (pH 8.5). The OH@Ti plates were immersed in the dopamine solution for 24 hours at room temperature. The dopamine-coated titanium substrates were then washed with distilled water and dried overnight at room temperature. The resulting substrates are referred to as **PDA@Ti**.

4. Preparation of MoS_2 coating

The MoS_2 nanoflakes assembled on the Ti plate were synthesized by a facile hydrothermal method. For the formation of MoS_2@Ti heterostructures, 0.186 mmol of sodium molybdate dihydrate ($Na_2MoO_4{\cdot}2H_2O$) and 1.20 mmol of thioacetamide (C_2H_5NS) were dissolved in 20 mL deionized water to make a transparent solution. This solution was then transferred to two separate Teflon-lined stainless-steel autoclaves. The KOH-etched Ti substrate was added to one autoclave, and the PDA-coated Ti substrate was added to the other. Both autoclaves were heated at 250 ℃ for 24 hours. The resulting dark brown solid product was dried at 80 ℃ for 12 hours to obtain MoS_2 coated Ti heterostructures. The resulting substrates are referred to as **MoS_2@Ti** and **MoS_2-PDA@Ti** for MoS_2 coated on the Ti plates and PDA-coated Ti plates, respectively.

5. Surface characterizations

The surface morphologies and elemental compositions of OH@Ti, PDA@Ti, MoS_2@Ti, and MoS_2-PDA@Ti substrates were analyzed using field emission scanning electron microscopy (FE-SEM, JSM-7001F, Hitachi High-Tech Corporation, Tokyo, Japan) equipped with an energy-dispersive X-ray spectroscopy (EDS) module. Powder X-ray diffraction (XRD) was performed using a Bruker D8 instrument (Karlsruhe, Germany) with Cu Kα radiation (λ = 0.15406 nm) to determine the structural properties and phase composition, scanning the 2θ range from 10° to 70°. Additionally, laser Raman spectrophotometry (inVia Reflex, Renishaw Co., Gloucestershire, UK) with a 532 nm excitation wavelength was employed for further analysis. The chemical bonding states of the elements were investigated using X-ray photoelectron spectroscopy (XPS, Multilab 2000, Thermo Fisher Scientific, Waltham, MA, USA). The surface wettability of the modified substrates was evaluated using a contact angle analysis system (DSA 25S, Kruss GmbH, Hamburg, Germany).

6. Cell viability test

The impact of the different samples on the proliferation of MG63 osteoblast-like cells was assessed using the MTT (3-(4,5-Dimethylthiazol-2-yl)-2,5-Diphenyltetrazolium Bromide) assay. MG63 cells, sourced from the Korean Cell Line Bank, were maintained in high-glucose Dulbecco's modified Eagle medium (Gibco™ DMEM, Fisher Scientific Inc., Waltham, MA, USA) enriched with 10% fetal bovine serum (Gibco™ FBS, Fisher Scientific Inc., Waltham, MA, USA), 100 units/mL penicillin, and 100 mg/mL streptomycin (32). The surface-modified Ti specimens were arranged in a 48-well plate and sterilized via UV irradiation for 30 minutes per side. MG63 cells were then seeded onto the sample surfaces at a density of 1×10^5 cells/well and incubated at 37 ℃ with 5% CO_2 . After 24 hours, MTT solution was introduced and incubation continued for an additional 3 hours. The culture medium was then removed, and 1 mL of dimethyl sulfoxide (DMSO) was added to solubilize the formazan crystals. Absorbance was measured using a Cytation3 Multi-Mode Reader (BioTek Instruments, Inc., Winooski, Vermont, USA). As a control, MG63 cells were also cultured in empty wells without specimens. Each MTT experiment was conducted in quintuplicate.

7. Electrochemical measurements

The corrosion resistance of the specimens was assessed using potentiodynamic polarization testing conducted on a Wonatech Zive SP2 potentiostat electrochemical system in a 0.9% NaCl solution. A typical three-electrode system was employed, consisting of a spiral platinum wire as the counter electrode, a Hg/HgO electrode as the reference electrode, and the specimens themselves serving as the working electrode. The area of the specimen exposed to the media was 1 cm^2. The potential range was set from -2.0 to 2.0 V with a scanning rate of 0.5 mV/s. The potential relative to the Hg/HgO electrode was converted to the potential of the reversible hydrogen electrode (RHE) using the Nernst equation (33):

$$E_{RHE} = EHg/HgO + 0.059 \times pH + 0.118$$

Electrochemical impedance spectroscopy (EIS) was carried out in the frequency range from 100 MHz to 100 kHz. All polarization tests were conducted five times to ensure reproducibility.

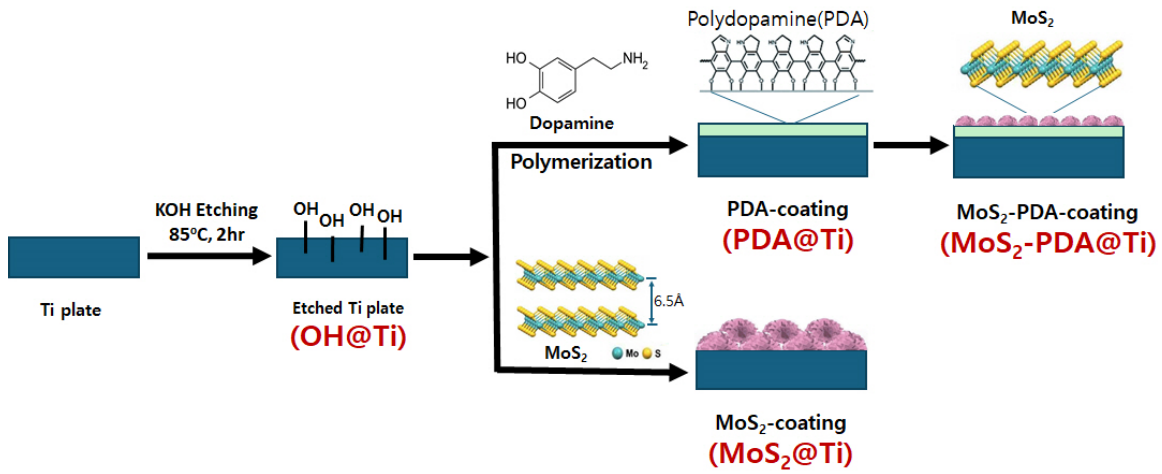

Figure 1. Schematic illustration of the surface modification procedure for titanium (Ti) plates. The process starts with KOH etching of Ti plates to introduce hydroxyl groups (OH@Ti), followed by polydopamine (PDA) coating through dopamine polymerization (PDA@Ti). The final step includes coating with molybdenum disulfide (MoS_2) either directly on the etched Ti plate (MoS_2@Ti) or on the PDA-coated Ti plate (MoS_2-PDA@Ti).

Results and Discussion

Figure 1 depicts the sequential modifications applied to titanium (Ti) plates to enhance their surface properties. The process begins with the etching of Ti plates using potassium hydroxide (KOH) at 85 ℃ for 2 hours, creating a thin, dense layer of titanium dioxide (TiO_2) enriched with hydroxyl (OH) functional groups (34), denoted as OH@Ti. This chemically modified surface serves as an excellent foundation for further coatings. Following the etching process, the Ti plates are coated with polydopamine (PDA) through the polymerization of dopamine on the OH@Ti surface, resulting in PDA-coated Ti (PDA@Ti). Subsequently, molybdenum disulfide (MoS_2) is synthesized directly on the PDA-coated Ti surface via a hydrothermal process involving molybdenum precursors, forming a dual-layer coating referred to as MoS_2-PDA@Ti. For comparative purposes, a control sample of MoS_2-coated Ti (MoS_2@Ti) is also prepared using the same hydrothermal conditions but without the intermediate PDA layer. This comprehensive modification strategy aims to enhance the surface properties of Ti plates for various applications, demonstrating the effectiveness of combining PDA and MoS_2 coatings.

1. Surface analysis

X-ray diffraction (XRD) analysis is employed to characterize the phase composition and crystal structure of the surface-modified titanium (Ti) samples, as depicted in Figure 2. Pristine titanium exhibits characteristic diffraction peaks at 2θ values of 35.2°, 38.7°, 40.3°, 53.2°, and 63.1°, consistent across all samples (indexed to JCPDS No. 89-4893) (35). The KOH treatment, intended to form a titanium hydroxide layer, does not show distinct peaks in the XRD pattern, suggesting minimal or undetectable changes in the crystalline structure. Similarly, the

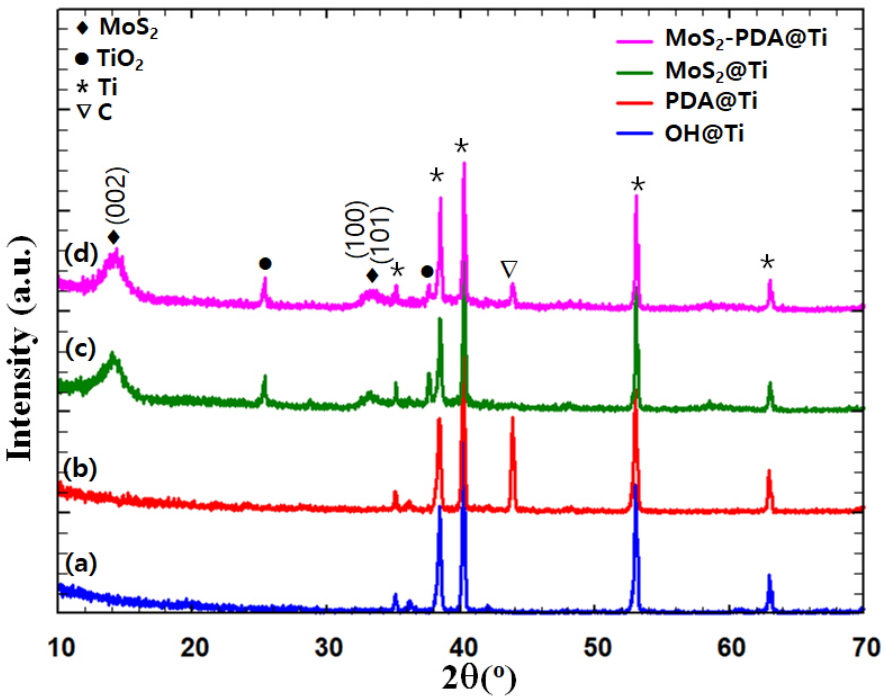

Figure 2. XRD patterns of surface-modified titanium (Ti) samples: (a) KOH-etched (OH). (b) polydopamine (PDA) coated. (c) molybdenum disulfide (MoS_2) coated. and (d) MoS_2-PDA coated. The symbols denote different phases: diamonds (♦) for MoS_2, circles (●) for TiO_2, asterisks (*) for Ti, and inverted triangles (▽) for carbon (C). Peaks are labeled with their corresponding planes.

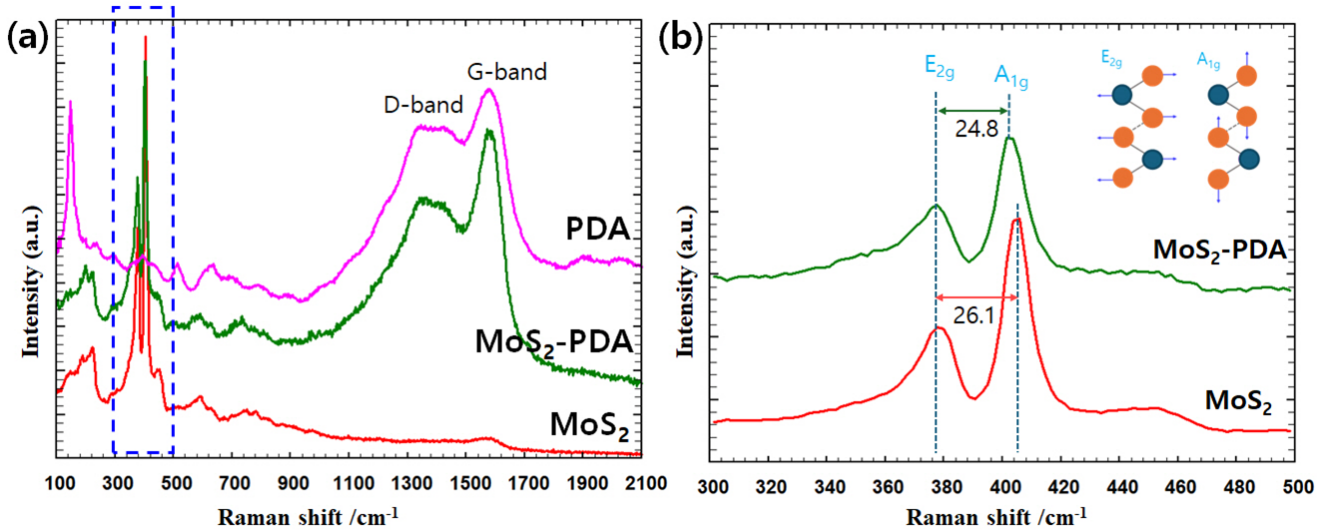

Figure 3. Raman spectra of surface-modified titanium (Ti) samples. (a) Raman spectra showing the D-band and G-band for polydopamine (PDA) coated, molybdenum disulfide (MoS_2) coated, and MoS_2-PDA coated samples. (b) Detailed view of the Raman spectra focusing on the E_{2g} and A_{1g} peaks for MoS_2 and MoS_2-PDA coated samples. The inset illustrates the vibrational modes corresponding to the E_{2g} and A_{1g} peaks.

PDA-coated Ti sample displays peaks nearly identical to those of the KOH-etched Ti, indicating that the PDA layer is either too thin or of insufficient quantity to significantly alter the crystalline structure. However, the appearance of a new peak at 2θ = 43.9° for PDA@Ti and MoS_2-PDA@Ti samples, attributed to carbon which are assigned to the (111) facet of diamond composition (indexed to JCPDS No. 50-1086) (35), suggests that the PDA coating may catalyze some graphitic diamond carbon formation, potentially due to PDA decomposition under the experimental conditions employed (36).

For MoS_2 coated samples, whether grown on PDA-coated Ti or directly on KOH-treated Ti, the XRD patterns display broad peaks at 14.3°, 33.0°, 39.5°, and 56.8°, corresponding to the (002), (100), (103), and (110) planes of MoS_2, respectively. These broad diffraction peaks are indexed to JCPDS No. 37-1492 (35), which corresponds to the hexagonal system with $P6_3/mmc$ as the space group. The broadening of these peaks suggests smaller crystallite sizes, typical for coatings rather than bulk materials, which is beneficial for enhancing the surface area crucial for various applications. It is worth noting that the MoS_2-PDA@Ti sample does not exhibit any additional peaks compared to the MoS_2@Ti sample, indicating that the PDA layer does not significantly influence the crystal structure of the overlaid MoS_2. This observation suggests that PDA primarily functions as a binding agent without altering the phase or crystalline nature of MoS_2.

Figure 3(a) exhibits the Raman spectra of PDA-coated Ti (PDA@Ti), MoS_2-coated Ti (MoS_2@Ti), and MoS_2-PDA-coated Ti (MoS_2-PDA@Ti) samples. In Figure 3(b), the spectra identify the E_{2g} mode, indicative of the in-plane vibrations of the two sulfur (S) atoms relative to the molybdenum (Mo) atom, and the A_{1g} mode, arising from the out-of-plane vibrations of the S atoms (37). The frequency difference ($\Delta\omega$) between these two modes serves as an indicator of the MoS_2 layer thickness (38). For the MoS_2-PDA@Ti sample, the $\Delta\omega$ value decreases to 24.8 cm^{-1}, compared to 26.1 cm^{-1} for the MoS_2@Ti

sample, suggesting a thinner MoS_2 layer has formed on the PDA-coated sample. Additionally, the Raman spectra exhibit the well known disorder-D (1367–1371 cm^{-1}) and graphite G (1595–1602 cm^{-1}) peaks in both PDA@Ti and MoS_2-PDA@Ti samples, confirming that the PDA layer remains intact after the subsequent coating of MoS_2. This indicates that the PDA coating does not peel off during the MoS_2 deposition process. The lower $\Delta\omega$ value and the preservation of the PDA layer demonstrate that applying a PDA coating can effectively control the growth of MoS_2, resulting in a finer and more uniform layer. This finding highlights the potential of PDA as a mediator in tailoring the properties of MoS_2 coatings for enhanced performance and integration on Ti implants.

The SEM image analysis highlights the morphologies of surface-coated materials on Ti surfaces, as supported by XRD data findings. Figure 4 presents detailed SEM images and corresponding EDS analyses for each modification sample. Figure 4(a) presents SEM images of KOH-etched Ti plates, revealing a rough, needle-like surface structure. EDS analysis shows a significant increase in oxygen content, confirming the presence of hydroxyl groups due to the KOH treatment. This textured surface likely enhances the adherence and interaction of subsequent coatings. Figure 4(b) presents SEM images of Ti plates coated with polydopamine (PDA) for 24 hours. Despite the PDA coating, the surface structure closely resembles that of the KOH-treated sample, indicating that the PDA conforms well to the underlying etched structure without significant morphological changes. This preser-

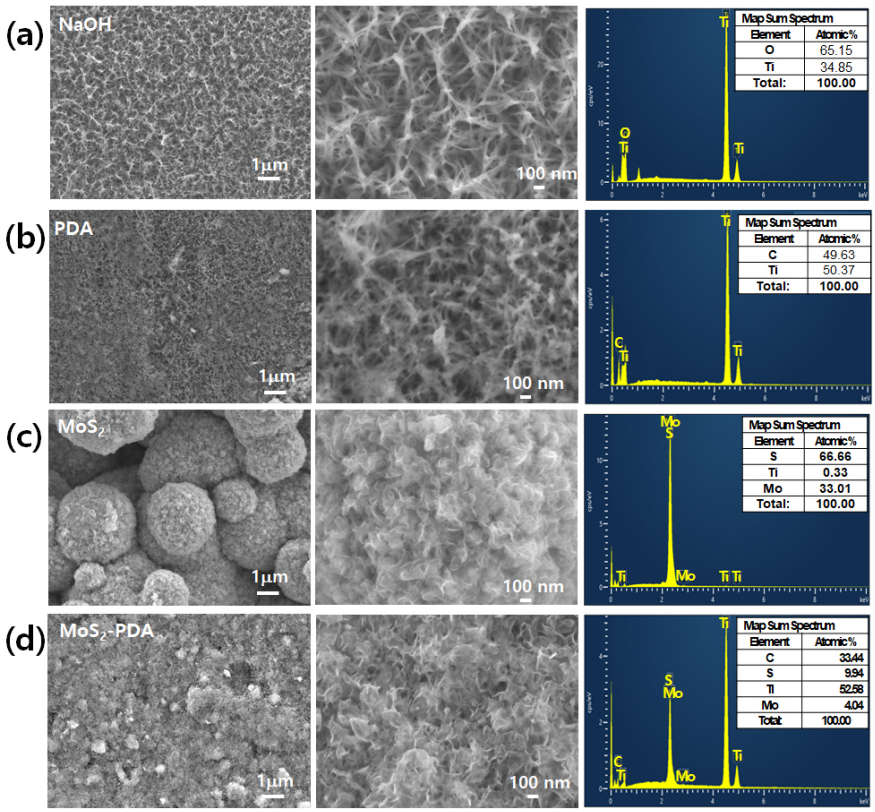

Figure 4. Scanning electron microscopy (SEM) images and Energy dispersive X-ray spectroscopy (EDS) analysis of surface-modified titanium (Ti) samples: KOH-etched Ti (OH@Ti), polydopamine-coated Ti (PDA@Ti), MoS_2-coated Ti (MoS_2@Ti), and MoS_2-PDA-coated Ti (MoS_2-PDA@Ti). The left and middle columns show SEM images at different magnifications (1 μm and 100 nm scale bars). The right column displays EDS spectra and the corresponding elemental compositions.

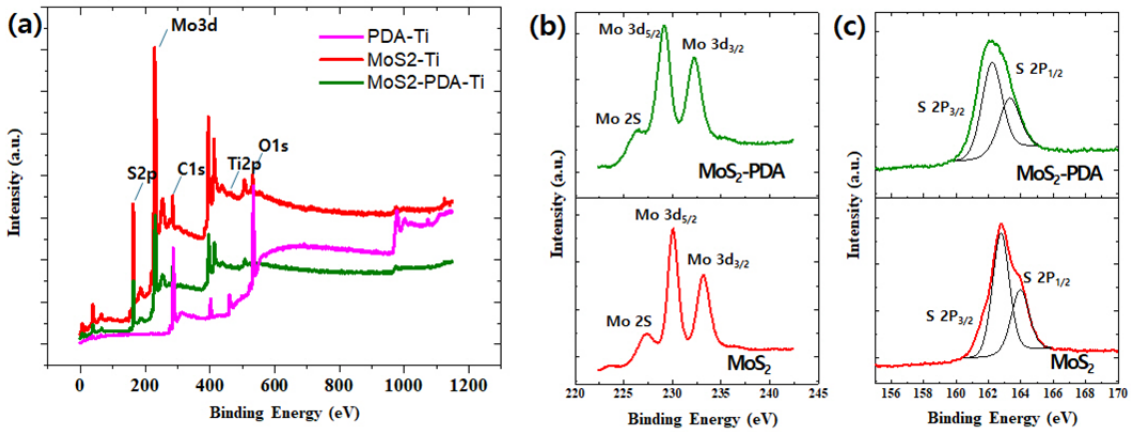

Figure 5. X-ray Photoelectron Spectroscopy (XPS) analysis of surface-modified titanium (Ti) samples: PDA-coated Ti (PDA@Ti), MoS_2-coated Ti (MoS_2@Ti), and MoS2@PDA-coated Ti (MoS_2-PDA@Ti). (a) survey XPS spectra. (b) High-resolution XPS spectra of the Mo 3d region. (c) High-resolution XPS spectra of the S 2p region.

Table 1. Elemental chemical compositions and ratios of different samples with XPS characterization.

	Ti 2p (%)	O 1s (%)	C 1s (%)	Mo 3d (%)	S 2p (%)	N 1s (%)
OH@Ti	31.12	51.30	17.58	-	-	-
PDA@Ti	5.28	26.06	62.55	-	-	6.11
MoS_2@Ti	-	7.86	20.83	26.76	44.55	-
MoS_2-PDA@Ti	-	9.16	27.46	23.47	38.69	1.22

vation of the textured morphology suggests effective adherence of the PDA to the rough surface. The increased carbon content, the major constituent of dopamine, is evident in the EDS analysis. Figure 4(c) and 4(d) depict Ti plates coated with MoS_2, applied directly on KOH-treated Ti (MoS_2@Ti) and on PDA-coated Ti (MoS_2-PDA@Ti), respectively. Both samples display a nanosheet-like structure characteristic of MoS_2. However, the presence of PDA hinders the growth of MoS_2 nanosheets, resulting in a more controlled and homogeneous distribution of MoS_2 on the PDA-coated Ti surface compared to the directly coated sample. EDS analysis reveals the presence of molybdenum, sulfur, and titanium, confirming the formation of MoS_2 within the composite material. For the MoS_2 directly coated on KOH-treated Ti, the decreased presence of Ti in the EDS suggests a substantial MoS_2 coating that effectively masks the underlying Ti. The controlled growth due to the presence of PDA suggests that the PDA layer not only adheres well to the underlying surface but also modulates the deposition of MoS_2, potentially enhancing electron transfer capabilities between MoS_2 and Ti. This could offer significant advantages in applications requiring efficient thermal management or enhanced electron conductivity. These SEM and EDS analyses provide crucial insights into the surface engineering of Ti, highlighting how different treatments influence the morphology and elemental composition of coatings.

In addition, XPS survey spectra of the PDA@Ti, MoS_2@Ti, and MoS_2-PDA@Ti samples were collected as shown in

Figure 5. As shown in Table 1, the increased amount of the O 1s peak in the KOH-treated surface indicates the formation of TiO_2 due to KOH treatment. This result is consistent with the SEM findings. After self-polymerization of the PDA film on KOH-etched Ti substrate, the intensity of the Ti 2p peaks remarkably decreased, while the C 1s peak increased and an additional N 1s peak appeared (listed in Table 1). It was observed that the Ti signal disappeared after the deposition of MoS_2, consistent with the SEM observations. The MoS_2@Ti and MoS_2-PDA@Ti samples exhibited detectable Mo and S peaks, confirming the presence of MoS_2, consistent with the reported values for MoS_2 crystals (17). For the MoS_2@Ti sample, the binding energies of Mo $3d_{3/2}$, Mo $3d_{5/2}$, S $2p_{1/2}$, and S $2p_{3/2}$ peaks are located at 233.2, 230.1, 162.8 and 161.7 eV, respectively. In the MoS_2-PDA@Ti, these peaks shifted to 232.4, 229.3, 162.4, and 161.6 eV, respectively, indicating a lower energy level compared to MoS_2@Ti due to electronic interactions between MoS_2 and PDA. In addition, nitrogen peaks at 399.9 eV were observed in the PDA@Ti and MoS_2-PDA@Ti samples, indicating the successful preparation of the PDA coating (39).

Figure 6 illustrates the surface wettability of various surface-modified titanium (Ti) samples. The KOH-etched Ti surface shows a low water contact angle of 18.46±1.3°, indicating significantly enhanced hydrophilicity due to the introduction of hydroxyl groups from the etching process (34). Polydopamine (PDA) coatings, while slightly reducing the hydrophilicity compared to KOH-treated samples, remain hydrophilic. In contrast, MoS_2 coatings are hydrophobic due to their S-Mo-S bonding characteristics. The contact angles of PDA@Ti and MoS_2@Ti are 48.58±4.1° and 101.03±3.3°, respectively (40). Interestingly, the MoS_2-PDA@Ti surface shows a contact angle of 83.77±2.2°, which is slightly lower than that of the MoS_2@Ti surface, suggesting that the PDA layer modestly improves the wettability of the surface.

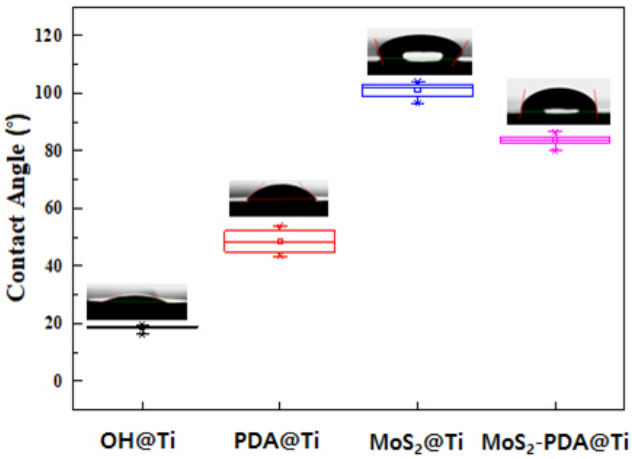

Figure 6. Water contact angles of the prepared titanium (Ti) samples with error bars representing the standard deviation (n = 5).

2. Cell viability analysis

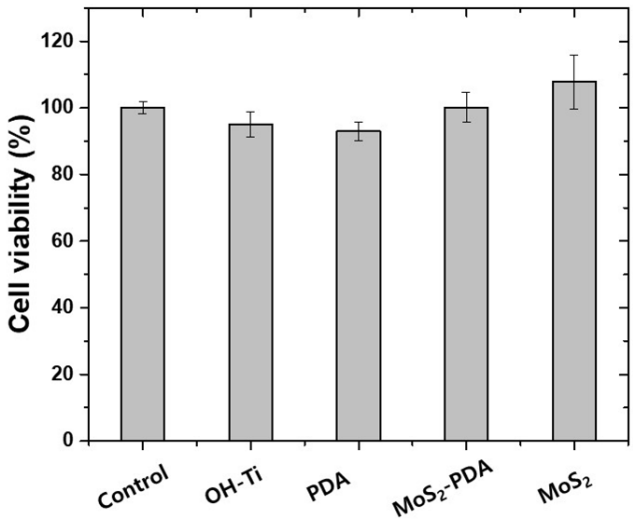

Figure 7. Cell viability of control and surface-modified titanium (Ti) samples. The data are expressed as percentages relative to the control, with error bars representing the standard deviation (n = 5).

Cell viability is determined using an optical analyzer and expressed as the percentage of viable cells relative to the total number of cells. This measurement is crucial for evaluating the biological activity of materials intended for medical applications (41). In this work, the MTT assay

against MG63 osteoblast-like cells is utilized to assess the response of cells on titanium (Ti) samples with various surface modifications. As shown in Figure 7, the minimum cell viability ratio is approximately 95.0±1.7% for KOH-etched Ti plates, 92.9±2.9% for PDA-coated Ti plates, about 107.8±8.2% for MoS_2-coated, and 100.1±4.5% for MoS_2-PDA-coated Ti plates, indicating no significant differences in cell viability between negative control cells and the cells grown on any of the specimens (P<0.05).

3. Electrochemical analysis

Various corrosion phenomena are observed across differently surface-modified titanium (Ti) samples, as depicted through Tafel polarization curves. The potentiodynamic polarization curves, conducted in 0.9% NaCl solution, are shown in the Figure 8(a), and the calculated corrosion potential (E_{corr}) and corrosion current (i_{corr}) are listed in Table 2 along with anodic and cathodic Tafel slope. The PDA@Ti sample demonstrates the highest corrosion resistance, indicated by its more noble corrosion potential of -0.04 V vs RHE and the lowest corrosion current density of 1.13 μA/cm^2. In contrast, the MoS_2@Ti sample exhibits a corrosion potential of -0.19 V vs RHE and a much higher corrosion current density of 39.63 μA/cm^2, indicating poor corrosion resistance compared to the other samples. Meanwhile, the MoS_2-PDA@Ti sample exhibits a corrosion potential of -0.06 V vs RHE with a corrosion current density of 22.54 μA/cm^2. While not as effective as PDA@Ti, this sample still shows improved corrosion resistance compared to MoS_2@Ti, suggesting that the combination of PDA and MoS_2 layers provides a synergistic effect in protecting the titanium substrate against corrosion.

The electrochemical properties are further explored through the electrochemical impedance spectroscopy (EIS). The Nyquist plot of EIS measurements in 0.9% NaCl solution, shown in Figure 8(b), serves as a tool for investigating the ion transport kinetics at the electrode-electrolyte interface (42). A smaller semicircle diameter in the plots indicates reduced resistance at the electrode-electrolyte interfaces, reflecting improved carrier transportation performance. Specifically, the Nyquist plot in Figure 8(b) reveals that the semicircle for MoS_2-PDA is smaller than that of PDA@Ti but larger than that of MoS_2@Ti. This indicates that the MoS_2-PDA@Ti sample strikes a balance by enhancing charge transfer characteristics compared to PDA@Ti but with slightly higher resistance compared to MoS_2@Ti. This highlights the nuanced role of the PDA interlayer in modulating

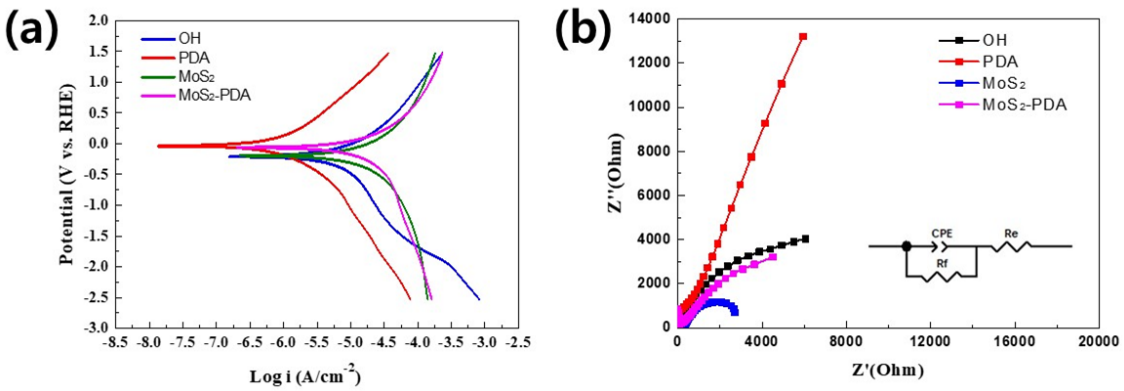

Figure 8. Electrochemical performance of surface-modified titanium (Ti) samples: (a) Tafel plots showing the polarization curves. (b) Electrochemical impedance spectroscopy (EIS) Nyquist plots, with the inset showing the equivalent circuit model used for fitting the data.

Table 2. Electrochemical parameters derived from Tafel plots for surface-modified titanium (Ti) samples. The parameters include corrosion potential (E_{corr}), corrosion current density (I_{corr}), anodic Tafel slope (βa), and cathodic Tafel slope (βc).

	E_{corr} (V vs RHE)	I_{corr} (A/cm^2)	βa (mV dec)	βc (mV dec)
OH@Ti	-0.21	10.27	125.87	-172.03
PDA@Ti	-0.04	1.13	937.44	-856.90
MoS_2@Ti	-0.20	39.63	247.48	-307.60
MoS_2-PDA@Ti	-0.06	22.54	161.14	-296.41

the electrochemical properties of MoS_2 coatings, contributing to both the corrosion resistance and the overall electrochemical performance of the titanium substrate.

The results of this study clearly demonstrate that the incorporation of a PDA interlayer significantly enhances the performance of MoS_2 bioactive coatings on titanium implants. This improvement is particularly evident in the controlled growth, enhanced surface properties, and increased corrosion resistance achieved. These findings provide an important foundation for maximizing the potential of MoS_2 coatings in dental and orthopedic implant applications. While the NIR-mediated antibacterial effects of MoS_2 are already well-known (43), this study highlights the necessity of evaluating the osteogenic potential of MoS_2-coated specimens in future research. By confirming whether these coatings not only prevent infections but also promote bone integration and regeneration, their applicability in orthopedic and dental implants could be greatly expanded.

Conclusions

This study investigates the surface modification of titanium (Ti) substrates using KOH etching, polydopamine (PDA), molybdenum disulfide (MoS_2), and a combination of MoS_2 and PDA (MoS_2-PDA). The results demonstrate that MoS_2-PDA coatings exhibit increased hydrophilicity and corrosion resistance compared to MoS_2 directly coated on Ti, highlighting the beneficial effect of the PDA interlayer. XRD, Raman spectroscopy, and SEM confirm the successful and uniform deposition of MoS_2 facilitated by PDA. Cell viability assays indicate high biocompatibility across all modified surfaces. Electrochemical impedance spectroscopy (EIS) reveals that MoS_2-PDA@Ti balances charge transfer characteristics, underscoring the role of PDA in enhancing electrochemical performance. The combination of MoS_2 and PDA coatings on Ti substrates presents a promising approach for enhancing surface properties, including corrosion resistance, wettability, and biocompatibility. The PDA interlayer plays a crucial role in controlling the growth and distribution of MoS_2, making it a valuable component in the surface engineering of Ti for advanced applications in biomedical implants and other technological fields.

Acknowledgements

This work was supported by the National Research Foundation of Korea grant funded by the Ministry of Science and the Korean Government (MSIP), Republic of Korea (No. 2021R1A2C1007407).

References

1. Zhang LC, Chen LY. A review on biomedical titanium alloys: Recent progress and prospect. Adv Eng Mater. 2019;21:1801215.
2. Abd-Elaziem W, Darwish MA, Hamada A, Daoush WM. Titanium-based alloys and composites for orthopedic implants applications: A comprehensive review. Mater Des. 2024;241:112850.
3. Liu Y, Rath B, Tingart M, Eschweiler J. Role of implants surface modification in osseointegration: a systematic review. J Biomed Mater Res A. 2020;108:470-84.
4. Narayana PSVS, Srihari PSVS. A review on surface modifications and coatings on implants to prevent biofilm. Regen Eng Transl Med. 2019;6:330-46.
5. Cui T, Wu S, Sun Y, Ren J, Qu X. Self-propelled active photothermal nano swimmer for deep-layered elimination of biofilm in vivo. Nano Lett. 2020;20: 7350-8.
6. Xu Y, Chen B, Xu L, Zhang G, Cao L, Liu N, et al. Urchin-like Fe3O4@Bi2S3 nanospheres enable the destruction of biofilm and efficiently antibacterial activities. ACS Appl Mater Interfaces. 2024;16:3215-31.
7. Cheeseman S, Christofferson AJ, Kariuki R, Cozzolino D, Daeneke T, Crawford RJ, et al. Antimicrobial metal nanomaterials: From passive to stimuli-activated applications. Adv Sci. 2020;7:1902913.
8. Han H, Yang J, Li X, Qi Y, Yang Z, Han Z, et al. Shining light on transition metal sulfides: New choices as highly efficient antibacterial agents. Nano Res. 2021;14:2512-34.
9. Shi J, Li J, Wang Y, Cheng J, Zhang CY. Recent advances in MoS_2-based photothermal therapy for cancer and infectious disease treatment. J Mater Chem B. 2020;8:5793-807.
10. Kwon MK, Lee JS, Kim ME, Choe HC, Surface characteristics and biocompatibility of mos_2-coated dental implant. Corros. Sci. Technol. 2024;23:72-81.
11. Hameed S, Sharif S, Ovais M, Xiong H. Emerging trends and future challenges of advanced 2D nanomaterials for combating bacterial resistance. Bioact Mater. 2024;38:225-57.
12. Xie M, Gao M, Yun Y, Malmsten M, Rotello VM, Zboril R, et al. Antibacterial nanomaterials: Mechanisms, impacts on antimicrobial resistance and design principles. Angew Chem Int Ed. 2023;62:e202217345.
13. Santos J, Moschetta M, Rodrigues J, Alpuim P, Capasso A. Interactions between 2D materials and living matter: A review on graphene and hexagonal boron nitride coatings. Front Bioeng Biotechnol. 2021;9:612669.
14. Yang X, Li J, Liang T, Ma C, Zhang Y, Chen H, et al. Antibacterial activity of two-dimensional MoS_2 sheets. Nanoscale. 2014;6:10126-33.
15. Kim TI, Kwon B, Yoon J, Park IJ, Bang GS, Park Y, et al. Antibacterial activities of graphene oxide-molybdenum disulfide nanocomposite films. ACS Appl Mater Interfaces. 2017;9:7908-17.
16. Yadav V, Roy S, Singh P, Khan Z, Jaiswal A. 2D MoS_2-based nanomaterials for therapeutic, bioimaging, and biosensing applications. Small. 2019;15: 1803706.
17. Yuan Z, Tao B, He Y, Liu J, Li C, Shen X, et al. Biocompatible MoS_2/PDA-RGD coating on titanium implant with antibacterial property via intrinsic ROS-independent oxidative stress and NIR irradiation. Biomaterials. 2019;217:119290.
18. Zhang G, Zhang X, Yang Y, Chi R, Shi J, Hang R, et al. Dual light-induced in situ antibacterial activities of biocompatible TiO_2/MoS_2/PDA/RGD nanorod arrays on titanium. Biomater Sci. 2020;8:391.
19. Li X, Zhu H. Two-dimensional MoS_2: properties, preparation, and applications. J Materiomics. 2015;1: 33-44.
20. Tang K, Wang G, Ruan Q, Peng F, Cao H, Chu PK. Controllable deposition of MoS_2 nanosheets on titanium by the vapor-phase hydrothermal technique

and comparison with the conventional liquid-phase hydrothermal method. Surf Coat Technol. 2020;404: 126497.
21. Shin MH, Baek SM, Polyakov AV, Semenova IP, Valiev RZ, Hwang WB, et al. Molybdenum disulfide surface modification of ultrafine-grained titanium for enhanced cellular growth and antibacterial effect. Sci Rep. 2018;8:9907.
22. Samy O, Zeng S, Birowosuto MD, El Moutaouakil A. A review on MoS_2 properties, synthesis, sensing applications and challenges. Crystals. 2021;11:355.
23. Omidiyan M, Srinoi P, Tajalli P, Lee TR. Review of light-activated antimicrobial nanoparticle-polymer composites for biomedical devices. ACS Appl Nano Mater. 2024;7:8377-91.
24. Feng Z, Liu X, Tan L, Cui Z, Yang X, Li Z, et al. Electrophoretic deposited stable chitosan@MoS_2 coating with rapid in situ bacteria-killing ability under dual-light irradiation. Small. 2018;14:1704347.
25. Chen X, Zhou J, Qian Y, Zhao L. Antibacterial coatings on orthopedic implants. Mater Today Bio. 2023;19: 100586.
26. Gnanasekar S, Kasi G, He X, Zhang K, Xu L, Kang ET. Recent advances in engineered polymeric materials for efficient photodynamic inactivation of bacterial pathogens. Bioact Mater. 2023;21:157-74.
27. Kim HJ, Kwon TY. Efficacy of polydopamine-coated titanium in order to improve bond strengths for dental resin cement. Korean J. Dent. Mater. 2017;44:179-86.
28. Lee JJ, Park IS, Shin GS, Lyu SK, Ahn SG, Bae TS, et al. Effects of polydopamine coating on the bioactivity of titanium for dental implants. Int J Precis Eng Manuf. 2014;15:1647-55.
29. Wang Y, Liu K, Huang K, Wei W, Huang Y, Dai H. Photothermal antibacterial MoS_2 composited chitosan hydrogel for infectious wound healing. Biomater Adv. 2024;156:213701.
30. Subramanian S, Campbell QT, Moser SK, Kiemle J, Zimmermann P, Seifert P, et al. Photophysics and electronic structure of lateral graphene/MoS_2 and metal/MoS_2 junctions. ACS Nano. 2020;14:16663-71.
31. Liu YL, Ai KL, Liu JH, Deng M, He YY, Lu LH. Dopamine-melanin colloidal nanospheres: an efficient near-infrared photothermal therapeutic agent for in vivo cancer therapy. Adv Mater. 2013;25:1353-9.
32. Kumar P, Nagarajan A, Uchil PD. Analysis of cell viability by the MTT assay. Cold Spring Harb Protoc. 2018;6:pdb.prot095505.
33. Kawashima K, Márquez RA, Son YJ, Guo C, Vaidyula RR, Smith LA, et al. Accurate potentials of Hg/HgO electrodes: Practical parameters for reporting alkaline water electrolysis overpotentials. ACS Catal. 2023;13: 1893-8.
34. Tanaka S, Hirose N, Tanaki T. Effect of the temperature and concentration of NaOH on the formation of porous TiO_2. J Electrochem Soc. 2005;152:C789-94.
35. Karlsruhe F. ICSD, Eggenstein-Leopoldshafen: Germany, 1998.
36. Roy R, Ravichandran D, Ravindranathan P, Badzian A. Evidence for hydrothermal growth of diamond in the C–H–O and C–H–O halogen system. J Mater Res. 1996;11:1164-8.
37. Ye M, Winslow D, Zhang D, Pandey R, Yap YK. Recent advancement on the optical properties of two-dimensional molybdenum disulfide (MoS_2) thin films. Photonics. 2015;2:288-307.
38. Lee C, Yan H, Brus LE, Heinz TF, Hone J, Ryu S. Anomalous lattice vibrations of single- and few-layer MoS_2. ACS Nano. 2010;4:2695-700.
39. Wang L, Shang X, Hao Y, Wan G, Dong L, Huang D, et al. Bi-functional titanium-polydopamine-zinc coatings for infection inhibition and enhanced osseointegration. RSC Adv. 2019;9:2892-905.
40. Fang LJ, Chen JH, Wang JM, Lin WW, Lin XG, Lin QJ, et al. Hydrophobic two-dimensional MoS_2 nanosheets embedded in a polyether copolymer block

amide (PEBA) membrane for recovering pyridine from a dilute solution. ACS Omega. 2021;6:2675-85.
41. Gerlier D, Thomasset N. Use of MTT colorimetric assay to measure cell activation. J Immunol Methods. 1986; 94:57-63.
42. Magar HS, Hassan RYA, Mulchandani A. Electrochemical impedance spectroscopy (EIS): Principles, construction, and biosensing applications. Sensors. 2021;21:6578.
43. Mu Z, Jin T, Chu T, Lu H, Chen Y, Li S, et al. Functionalized MoS_2-nanosheets with NIR-triggered nitric oxide delivery and photothermal activities for synergistic antibacterial and regeneration-promoting therapy, J. Nanobiotechnology. 2023;21:463.

Original Article

Effect of MoS_2/polydopamine coating on surface properties and biocompatibility of Ti implants

Minseo Yu[1], Yo Han Song[2], Mi-Kyung Han[1,]*

[1]*Department of Materials Science and Engineering, Chonnam National University, Gwangju, Republic of Korea*
[2]*Department of Chemistry, Gwangju Institute of Science and Technology (GIST), Gwangju, Republic of Korea*

This study investigates the role of polydopamine (PDA) as an intermediate layer for enhancing the adhesion, surface properties and corrosion resistance of molybdenum disulfide (MoS_2) coatings on titanium (Ti) implants. Two approaches are compared: one involving direct MoS_2 coating on Ti and the other involving MoS_2 coating on PDA-treated Ti surfaces. The modified surfaces are comprehensively characterized using X-ray diffraction (XRD), X-ray photoelectron spectroscopy (XPS), Raman spectroscopy, and scanning electron microscopy (SEM). Characterization results from Raman spectroscopy and SEM confirm that the PDA layer facilitates more uniform and finely structured MoS_2 coatings. Wettability tests demonstrate that MoS_2-PDA-treated surfaces exhibit improved hydrophilicity compared to direct MoS_2 coatings. Corrosion resistance tests using potentiodynamic polarization reveal that MoS_2-PDA-treated samples show a lower corrosion current density and more noble corrosion potential compared to directly coated MoS_2 samples. Cell viability assays show comparable biocompatibility for both MoS_2-PDA-treated and direct MoS_2-coated surfaces, with a slight preference for the MoS_2 group in terms of cell compatibility. These findings suggest that while the PDA interlayer improves structural and surface properties, further studies are needed to fully understand the biocompatibility differences between the two approaches. The PDA interlayer still shows promise in enhancing surface properties and corrosion resistance for potential orthopedic applications.

Keywords : MoS_2 coating, Dopamine, Wettability, Cell viability, Titanium dental implants